Dalton Transactions

ROYAL SOCIETY OF CHEMISTRY

PAPER

View Article Online
View Journal | View Issue

Cite this: *Dalton Trans.*, 2026, **55**, 7685

Effect of lanthanide(III) complexation on the radiolytic stability of Macropa

Alexandre Gaspar, [a] Julie Hostier,[a] Dominique Guillaumont, *[a] Claude Berthon, [a] Xavier Hérès, [a] Luca Briscese,[a] Bertrand Kuhnast [b] and Laurence Berthon *[a]

Received 19th March 2026,
Accepted 22nd April 2026

DOI: 10.1039/d6dt00671j

rsc.li/dalton

The growing use of radionuclides in nuclear medicine for therapy and diagnosis requires the development of chelators that combine high complexation performance with strong radiolytic stability. Macropa, an ether-crown ligand, displays a strong affinity for large trivalent cations and can be used as a chelator for radionuclides such as ^{225}Ac, $^{149/161}$Tb, and $^{132/135}$La. Here, we investigated the γ-radiolysis of Macropa in water and evaluated the impact of complexation by studying Ln-Macropa complexes. Samples were irradiated up to 30 kGy, and degradation was monitored by ESI-MS and HPLC-ESI-MS, while quantification was made by ^{1}H NMR. For free Macropa, the major degradation pathways involve carbon–carbon bond cleavages and the loss of the picolinate arm, together with additional minor hydroxylated and unsaturated products. In contrast, Ln-Macropa complexes mainly form hydroxylated products arising from HO$^{\bullet}$ attack, and no La decomplexation was detected. Radiolytic degradation yields indicate that Macropa is already highly resistant ($G_0 \approx -1.25 \times 10^{-7}$ mol J^{-1}) and that complexation with La further enhances stability ($G_0 \approx -0.76 \times 10^{-7}$ mol J^{-1}). DFT calculations (BDE and Fukui indices) support these observations by showing increased C–C bond strengths upon La(III) complexation, as well as a shift in atomic positions most susceptible to radical attack from the crown ether to the pyridine ring of the carboxylate arm. Overall, these results highlight Macropa as a robust chelator under γ-irradiation and show that complexation can both improve stability and change degradation pathways toward products that preserve the ligand's chelating functions.

Introduction

Nuclear medicine is a rapidly expanding field of research that relies on the use of radionuclides for both diagnosis and therapy of diseases such as cancer. In the latter case, α, β$^-$ and auger electron emitters are employed to damage the DNA of cancer cells through their highly energetic, short-range emissions. This localized effect necessitates the vectorization of radionuclides to the tumor site.[1] In addition, a chelating agent is required during transport to prevent any untargeted release of the radionuclide into the biological environment. Several radionuclides are currently being investigated for therapeutic applications, including ^{225}Ac, $^{149/161}$Tb, and $^{132/135}$La.[2–8] Finding a chelating agent that can withstand the radiation emitted by the radionuclide, and understanding the mechanisms involved, is one of the key challenges that must be addressed.

Several chelators are currently being investigated in clinical trials, with DOTA considered as the gold standard for trivalent cation chelation. Despite its status as the reference chelator in nuclear medicine, its limitations prevent it from being considered an ideal chelating agent.[2,9–15] To overcome certain constraints, such as slow complexation kinetics, the need for prolonged heating during complex formation, and the risk of transmetallation, new families of cyclic chelators have been developed, particularly those derived from 18-crown-6 ethers. Among these next-generation chelators, H_2Macropa (*N*,*N*′-bis[(6-carboxy-2-pyridyl)methyl]-4,13-diaza-18-crown-6), (Fig. 1) has distinguished itself by its ability to complex radionuclides such as ^{225}Ac and ^{213}Bi.[7] In contrast to DOTA, complexation can be achieved at room temperature in less than 10 minutes.[16,17] The complex formed with ^{225}Ac also demon-

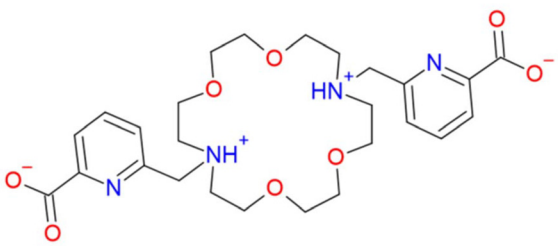

Fig. 1 Schematic representation of Macropa. For simplicity's sake, Macropa is portrayed as neutral form (pH 4.5).

[a]*CEA, DES, ISEC, DMRC, Univ Montpellier, Marcoule, France.*
E-mail: laurence.berthon@cea.fr, dominique.guillaumont@cea.fr
[b]*Paris-Saclay University, CEA, CNRS, Inserm, BioMaps, SHFJ, Orsay, 91401, France*

strated excellent stability in solution, remaining intact for at least one week.[15] Finally, *in vivo* studies revealed no undesirable accumulation in organs.[15]

Macropa forms highly coordinated complexes (10–11 coordination sites) with large trivalent cations such as La^{3+}. The cation is embedded within the macrocyclic cavity, coordinated by ten internal donor atoms (four N and six O) arranged in a pseudo-bicapped antiprismatic geometry. Macropa can adopt different conformations.[18] For large cations such as La, the macrocycle preferentially adopts the Δ(δλδ)(δλδ) conformer, a more open configuration that allows an additional water molecule to bind at the eleventh coordination site.[18–21] In contrast, for smaller cations such as Tb^{3+}, the ligand favors the Δ(λδλ)(λδλ) conformer, which generally leads to a reduced coordination number.[15,20] The complexation constants K of Macropa with the lanthanide series show that $\log K$ values are higher for the lighter elements, which have larger ionic radii. For instance, $\log K$(La-Macropa) is around 14–15, whereas $\log K$(Lu-Macropa) drops to about 7–8.[20,22] This trend is also observed for actinides, with an even higher selectivity across the series.[23] Thus, Macropa exhibits an inverse size-selectivity trend compared to DOTA, preferentially stabilizing complexes with larger ionic radii.

The effect of metal ion complexation on radiolytic stability has already been investigated, particularly for extractants used for nuclear fuel reprocessing.[24–31] These studies have shown that metal complexation can alter the radiolytic stability of extractants.[29–33] More recently, studies have focused on the DOTA chelator in aqueous solution.[34–36] A study by Mahti *et al.* showed that when DOTA is complexed with zirconium(IV) in aqueous media, its radiolytic stability is significantly increased.[34] In addition, work by Avraham *et al.* demonstrated that the reactivity of certain radicals generated by radiolysis of water changed when DOTA was complexed to Ce(III).[35] Beyond this stabilizing effect, a modification of the degradation pathway was also observed. It was shown that free DOTA degrades mainly by loss of an acetate arm or by loss of CO_2, whereas M-DOTA complexes degrade mainly by oxidation, leading to the addition of an OH group in the system.[34]

To the best of our knowledge, the radiolytic stability of Macropa has not yet been investigated. This aspect is nevertheless crucial, especially for therapeutic applications, since radionuclides used in therapy can have half-lives of several days. For example, the activity of a ^{225}Ac-labelled radiopharmaceutical would typically be about 10 MBq in 1 mL.[38] Therefore, the chelator bound to actinium is subjected to a dose rate of approximately 0.16 kGy h^{-1}. Roughly, after 24 hours, the chelator would have absorbed a dose of about 4 kGy. It is therefore important to identify the species formed during radiolysis. This study aims to extend the understanding of the γ-radiolysis behaviour of Macropa and the influence of metal complexation. Two complexes, La-Macropa and Tb-Macropa were investigated in order to assess the impact of complexation on the stability of the system in water. The degradation products were identified by mass spectrometry (HPLC-ESI-MS), and degradation pathways are proposed. The degradation of the Macropa and La-Macropa were quantified by ^{1}H NMR. In addition, Density Functional Theory (DFT) calculations were performed to compare the bond strength between free Macropa and the La-Macropa complex and to identify the atomic positions most susceptible to be attacked by radicals present in water.

Experimental section

Chemicals

Solid Macropa (H_2bp18c6) was purchased from MedChemExpress Europe (purity >99%). Solid lanthanum(III) chloride heptahydrate and terbium(III) chloride hexahydrate were obtained from Sigma-Aldrich (purity >99.9%). All commercial products were used as received without further purification. pH of the solutions was measured with a pH electrode (Metrohm) calibrated against standard buffers.

Synthesis and characterization of M(III)-Macropa

The Macropa complex was synthesized using a 1 : 1 metal : ligand ratio. Solid Macropa was dissolved in water (5×10^{-3} mol L^{-1}), lanthanum(III) chloride heptahydrate and terbium(III) chloride hexahydrate were subsequently added to the solution. pH was adjusted above 5 with NH_4OH 30%. The pH of the solutions was measured using a Metrohm pH electrode calibrated against standard buffers. The pH was set close to 5 to approximate the pH of Macropa in water and to favour complexation. The mixture was stirred for 10 minutes at room temperature. Complete complexation was confirmed by ESI-MS and ^{1}H NMR (Fig. S1 and S2).

Irradiation experiments

Aqueous solutions of Macropa and Ln-Macropa (5×10^{-3} mol L^{-1}) were irradiated with γ-radiation using a GRS-D1 Gamma-Service-Medical-GmbH irradiation system at CEA Marcoule. It uses a calibrated ^{137}Cs source with a dose rate of 0.6–0.7 kGy h^{-1}. Dosimetry was performed using the Fricke method.[37] Therefore, two milliliters of each sample were prepared and irradiated for 5 to 48 hours, corresponding to doses of approximately 4, 9, 20, and 30 kGy. The absorbed doses, irradiation times, and pH values of the irradiated samples are summarized in Table 1.

Once the irradiation was completed, all samples were stored in a freezer until analysis over the following days. For each analysis, the samples were thawed only for the duration of the measurement and then immediately refrozen until the next analysis.

Mass spectrometry

Samples were diluted at a concentration of 2.5×10^{-4} mol L^{-1} in pure H_2O and analysed with a micrOTOF-Q II (Bruker Daltonik GmbH, Bremen, Germany) electro-spray ionization (ESI) quadrupole time-of-flight (TOF) mass spectrometer calibrated daily using an Agilent (G1969-85000) ESI Low Concentration Tuning Solution. Samples were injected at a

Table 1 Irradiation conditions for 5 mM Macropa and La-Macropa solutions in water

Sample name	Dose rate (kGy h^{-1})	Irradiation time (h)	Dose (kGy)	pH
Macropa	0	0	0	5.2
	0.89	5h00	4.5	4.7
	0.87	10h00	8.7	4.6
	0.86	23h55	20.5	4.1
	0.80	33h05	26.3	4.0
La-Macropa	0	0	0	6.0
	0.70	6h17	4.4	4.8
	0.71	13h50	9.8	4.7
	0.72	29h20	21.0	4.5
	0.64	46h18	29.6	4.3
Tb-Macropa	0	0	0	6.2
	0.65	6h17	4.1	5.7
	0.63	13h50	8.7	5.4
	0.66	29h20	19.3	4.9
	0.63	47h13	29.8	4.6

flow rate of 180 μL h^{-1} by syringe pump. The experimental conditions were as follows: positive ion mode, ion spray voltage of 4500 V, IsCID 0 eV, N_2 as drying and nebulizing gas, 4 L min^{-1}, 0.3 bar, 200 °C. Low mass tuning method was used, which allowed the analysis of Macropa and Ln-Macropa fragments. Compass Data Analysis software (Bruker Daltonics) was used for data processing. Species were identified by comparing an experimental isotopic pattern with a simulated one using DataAnalysis 4.2 software.

HPLC

Isocratic HPLC analysis was done by using the Thermo Fischer Ultimate 3000 HPLC System with vacuum degasser and pumps. Isocratic elution was carried out with a mobile phase (Milli-Q water + 0.1% formic acid)/acetonitrile 8 : 92 v/v. An amount of 100 μL of sample was loaded thanks to an injection valve of 3.4 μL into an InfinityLab Poroshell 120 HILIC-Z column (150 mm × 2.1 mm, 2.7 μm, Agilent) at a flow rate of 0.200 mL min^{-1} over 10 min for La-Macropa solutions. The concentration of the injected solutions varied between 0.005 and 0.05 mmol L^{-1}. Samples were diluted 10 times in a 90 : 10 acetonitrile : H_2O before analysis. Before the measurement of each sample, a 'blank' sample is recorded with injection of ACN.

Nuclear magnetic resonance

Analyses were performed at 298 K with an Agilent DD2 400 MHz spectrometer equipped with a 5 mm OneNMR probe. To avoid dilution, an internal tube containing the deuterated reference solvent (CD_3CN or acetoneD6) was surrounded by the tube containing the sample in pure H_2O. All spectra were normalized with the reference solvent used as external standard.

The ^1H NMR water signal was presaturated to enhance signals intensity of our compounds. OpenVnmrJ 4.2 software was used for data acquisition and ACDLABS 12.0 Chemsketch software for data processing.

Computational methods

Density functional theory (DFT) calculations were conducted using Gaussian 16 for Macropa and La(III)-Macropa complex.[41]

Optimized geometries were verified as true minima through frequency calculations, with no imaginary frequency detected. Zero-point energies, along with thermal corrections at 298.15 K, were obtained from frequency calculations and added to the electronic energies. The 6-31G+(d,p) basis set was applied to H, C, N, and O atoms. For lanthanum, the ECP46MWB Stuttgart–Cologne quasi-relativistic effective core potential was used to represent core electrons, along with the corresponding basis set for valence electrons.[42] The bond dissociation energy (BDE) is defined as the reaction enthalpy for the homolytic dissociation of a bond, represented by the following reaction:

$$R - X \rightarrow R^{\bullet} + X^{\bullet} \quad (1)$$

The BDE of an R–X bond is calculated as the difference in enthalpies of each species involved in this homolytic reaction:

$$E_{BDE} = \Delta_f H^{\circ}_{298.15\,K}(R^{\bullet}) + \Delta_f H^{\circ}_{298.15\,K}(X^{\bullet}) - \Delta_f H^{\circ}_{298.15\,K}(R - X) \quad (2)$$

In line with previous Zr-DOTA studies,[34] the hybrid density functional B3P86, was used to optimize geometrical parameters and compute BDEs.[43,44] All BDEs calculations were done in the gas phase.

The Fukui function characterizes the change in electron density resulting from the addition or removal of an electron. It enables the prediction of molecular sites that are most reactive toward nucleophilic, electrophilic, or radical attacks.

In this work, the Condensed Fukui indices have been determined to get a quantitative description of the local reactivity of an atom.[45,46] The radical Fukui indice $f^{0,\alpha}$ for an atom α is defined as follows:

$$f^{0,\alpha} = \frac{1}{2}[q^{\alpha}_{N-1} - q^{\alpha}_{N+1}] \quad (3)$$

where q^{α} is the partial charge on the atom α. q^{α}_{N+1} is the partial charge of atom α when adding one electron to the molecule, whereas q^{α}_{N-1} corresponds to the partial charge of the atom when removing one electron from the molecule. In this approach, atoms with the highest f^0 values are expected to be the most susceptible to radical attack. Partial charges were derived from a Natural Population Analysis (NBO).[47]

Results and discussion

Identification of irradiated Macropa and Ln(III)-Macropa degradation products

Aqueous solutions of Macropa and Ln-Macropa were irradiated with γ-radiation up to 30 kGy. Those irradiation doses were chosen for evaluating the stability of chelator prior to injection, enabling the characterization of radiolysis products at

low concentrations.[9,38–40] ESI-MS analysis of 5×10^{-3} mol L^{-1} irradiated samples in water were performed before and after irradiation. With increasing dose, the abundance of Macropa and Ln-Macropa ions are decreasing, while degradation products signals are increasing.

For Macropa samples (pH of 5.2 before irradiation), the characteristic ion at m/z = 533 (species A, $[MacropaH]^+$) was observed (Fig. 2). At 0 kGy, an additional species at m/z = 398 (species **B**) is also detected. This species corresponds to Macropa after the loss of one picolinate arm. Since the 0 kGy Macropa solution was kept at room temperature during the irradiation of the other samples, this product likely arises from hydrolysis of the compound. This compound is not observed by ESI-MS in a freshly prepared solution. It is worth nothing that due to the presence of carboxylate groups, sodium or potassium adducts can form readily in place of a proton (Fig. S12). Upon irradiation from 4.5 to 26.3 kGy, new ions appeared at m/z = 354 and 372, corresponding to degradation products (species **C** and **D**). The abundance of species **B** also increases with increasing dose. Species **C** (m/z = 354) results from the loss of a CO_2 group from species **B**, and species **D** corresponds to the addition of one oxygen atom to the molecular structure of species **C**. The last degradation product at m/z = 531 (species **E**), is assigned to the formation of a double bond in the system. The position of this double bond will be discussed in the theoretical chemistry section.

Upon irradiation, a decrease in pH from 5.2 to 4.0 is also noted. This decrease is likely due to the release of H^+ ions during Macropa degradation.

The Macropa solution was also analysed by HPLC-ESI-MS (chromatogram in Fig. S10). Species **A** to **E** were observed. The chromatogram also reveals the formation of a species **F** at m/z = 507 corresponding to Macropa $-CO_2$ +OH whose abundance was too low to be detected by direct ESI-MS alone. All degradation products are summed up in Fig. 2 and a simplified degradation pathway for Macropa is proposed in Fig. 3.

For La-Macropa and Tb-Macropa samples, the identification of the degradation products were carried out based on ESI-MS spectra. The spectra for the irradiated solutions of La-Macropa up to 30 kGy are presented in Fig. 4.

At 0 kGy, an ion corresponding to species **A′** ($[La\text{-}Macropa]^+$) is observed. It corresponds to a complex involving doubly deprotonated Macropa and La^{3+}. From 4.0 to 30.0 kGy, the peak of the complex **A′** is still present at its expected m/z value, while additional peaks corresponding to degradation products **B′**, **C′**, **D′**, **E′** and **F′** appear at m/z = +16, +32, +48, +14 and −26 from species **A′**, respectively.

The primary ion **B′** is La-Macropa with an oxygen atom added on the complex. It is already present at 5 kGy. Heavier products **C′** and **D′**, also correspond to the addition of two or

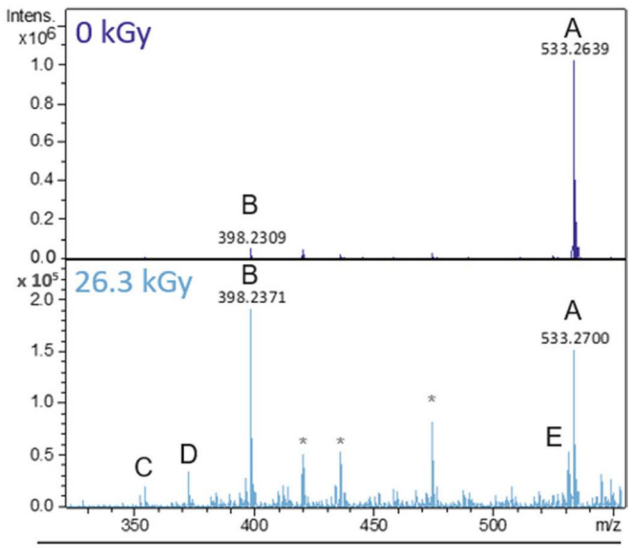

m/z	Species
A : 533.3	Macropa
B : 398.2	Loss of picolinate arm
C : 354.2	Loss of CO_2 on Species B
D : 372.2	Addition of O on Species C
E : 531.2	Formation of a double bond
F : 507.3	Loss of CO_2 and addition of O on Macropa
* Adducts : 420, 436, 474	Adducts with Na^+ and K^+

Fig. 2 Top: ESI-MS spectra of 5×10^{-3} mol L^{-1} γ-irradiated Macropa samples diluted 20 times in water. Bottom: main degradation products observed for Macropa samples based on HPLC and ESI-MS spectra. Adducts are detailed in Fig. S12.

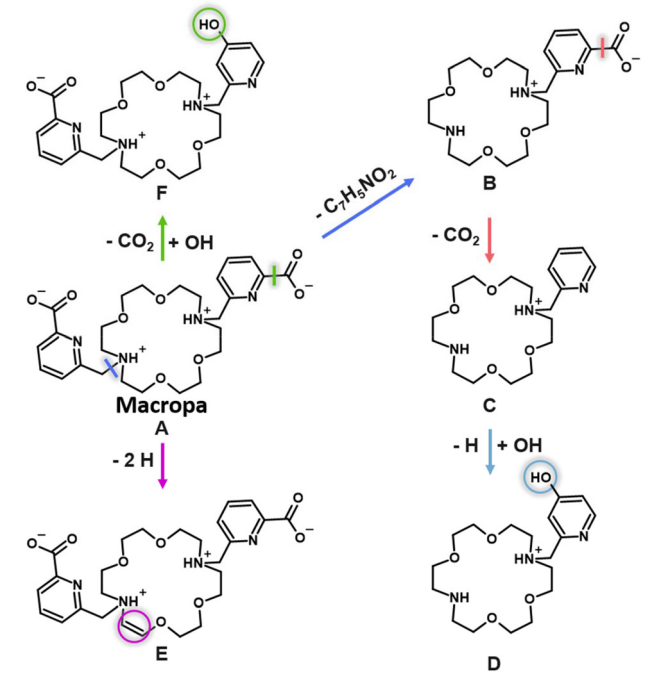

Fig. 3 Simplified degradation pathway for Macropa γ-radiolysis in pure water.

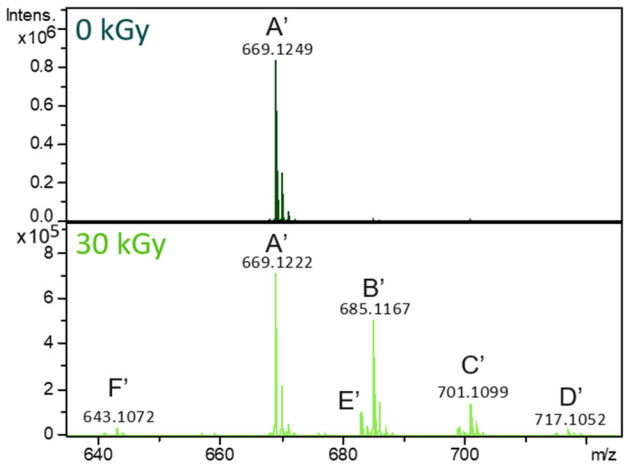

m/z	Species
A′ : 669.1	La-Macropa
B′ : 685.1	Addition of O on Species A′
C′ : 701.1	Addition of O on Species B′
D′ : 717.1	Addition of O on Species C′
E′ : 683.1	Formation of a double bond on Species B′
F′ : 643.1	Loss of CO_2 on Species B′

Fig. 4 Top: ESI-MS spectra of 5 × 10^{-3} mol L^{-1} γ-irradiated La-Macropa samples diluted 20 times in water. Bottom: main degradation products observed for La-Macropa samples based on HPLC and ESI-MS spectra.

three oxygen atoms on the La-Macropa complex. Based on HPLC-ESI-MS analysis (Fig. S11), several forms of those species, with the OH group added either to the picolinate arm or to the ether-crown backbone, may be possible. Species **E′** could correspond either to the formation of a C=O bond or to OH addition combined with the formation of a double bond. Based on the NMR results (discussed later), this fragment addition is proposed to occur on the aromatic ring of the picolinate arm, making C=O formation unlikely. No species corresponding to the formation of a double bond was detected in ESI-MS or HPLC-ESI-MS (Fig. S11 and S13). Therefore, it is hypothesized that product **E′** originates from species **B′**, which was already observed at 5 kGy followed by the formation of the double bond. In the same way, the ion **F′** corresponds to the loss of CO_2 on species **B′**.

All degradation products are summarized in Fig. 4 and a simplified degradation pathway of La-Macropa is proposed Fig. 5. The structures of species **B′**, **C′**, **D′** and **E′** are unknown based on the mass spectra but were tentitavely assigned using DFT calculations. The proposed structures will be discussed in the next section.

The ESI-MS spectra of irradiated Tb-Macropa samples are given in Fig. S14. The results show a similar behavior to that of the La-Macropa system. However, degradation products corresponding to species **D′** and **E′** were not detected in sufficient

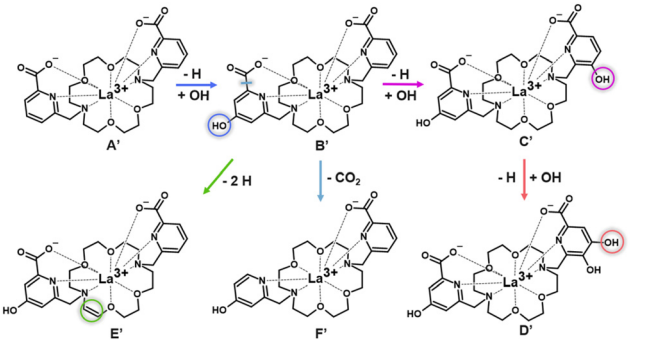

Fig. 5 Simplified degradation pathway for La-Macropa γ-radiolysis in pure water.

amounts to be considered present. Moreover, although ESI-MS is not a quantitative method, it can be noted that the **B′**/**A′** ratio is higher for La-Macropa than for Tb-Macropa. In contrast, the **F′**/**A′** ratio is higher for the Tb-macropa complex. These subtle differences may reflect metal-dependent stability trends.

For both irradiated La- and Tb-Macropa complexes, we can observe degradation products that differ from those obtained for free Macropa. In the case of free Macropa, bond cleavages within the pendant arms are mainly observed. As a result, the number of coordinating functions, and therefore the complexation properties of the ligand, might decrease. In contrast, for the Ln-Macropa complexes, the main degradation products correspond to the addition of fragments (+OH) to the ligand. As a result, the coordinating functions are preserved. This modification is most likely initiated by a $HO^{\bullet}$ radical attack, generating a Macropa-$HO^{\bullet}$ radical intermediate. A second radical present in solution can then abstract a hydrogen atom from this intermediate, leading to either H_2 or H_2O, and yielding the final Macropa-OH degradation product (eqn (5)).[28,34,36,48,49]

$$\text{Macropa} + OH^{\bullet} \rightarrow \text{MacropaOH}^{\bullet} \quad (4)$$

$$\text{MacropaOH}^{\bullet} + H^{\bullet}/HO^{\bullet} \rightarrow \text{MacropaOH} + H_2/H_2O \quad (5)$$

The formation of oxidation products bearing additional OH groups has also been reported for DOTA[34,36] and may impact the complexation constants. Also, the pH of Ln-Macropa solutions slightly decreases upon irradiation, most likely due to the release of protons following the addition of $HO^{\bullet}$ radicals to the ligand. The pH decrease might favour decomplexation of the cation locally. For these reasons, it is important to quantify the amount of non-degraded complex and compare it with free Macropa, in order to determine what fraction of the complex retaining its properties is left after irradiation.

Quantitative analysis of La(III)-Macropa and Macropa degradation

In order to quantify the degradation of La-Macropa and Macropa, ^{1}H NMR spectra of irradiated solutions have been recorded. Based on previous studies by Blei *et al.*[20] we per-

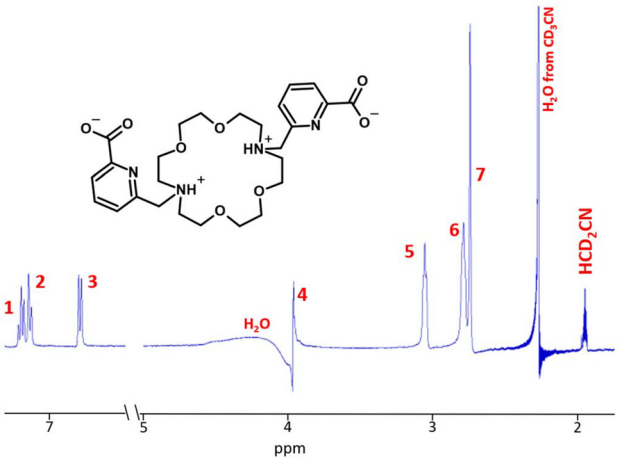

Fig. 6 ^{1}H NMR spectra of non-irradiated Macropa solution. Conditions: Macropa 5 × 10^{-3} mol L^{-1} in pure water (pH = 5.2), 25 °C. CD_3CN is used as external lock solvent and residual undeuterated signal to normalize spectra.

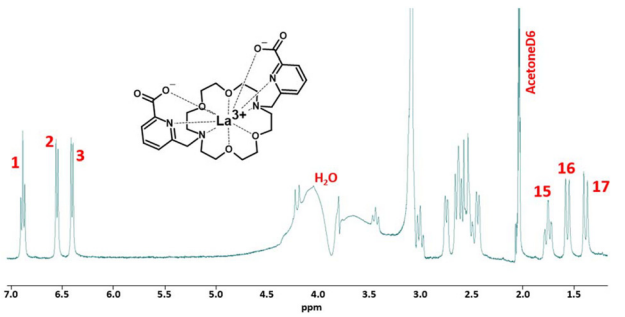

Fig. 7 ^{1}H NMR spectra of non-irradiated La-Macropa solution. Conditions: La-Macropa 5 × 10^{-3} mol L^{-1} in pure water (pH = 6.0), 25 °C. AcetoneD6 is used as external lock solvent and residual undeuterated signal to normalize spectra. Attribution is detailed in SI.

formed the measurements at 25 °C to obtain the spectra shown in Fig. 6 and 7.

The ^{1}H NMR spectra was also recorded for Tb-Macropa but is difficult to interpret because of Tb paramagnetic effects. The results are given in Fig. S18 to S21 but will not be discussed further.

For La-Macropa, the assignment of spectral peaks is given in Fig. S3–S9. Signals 1 to 3 were identified as the aromatic protons on the picolinate arms in both systems. Signal 4 was assigned to the proton on the carbon atom of the methylene bridge between the picolinate arm and the crown-ether ring. Because this signal partially overlaps with the water peak, it was not considered for further quantitative analysis. The remaining signals correspond to protons of the crown-ether (Fig. S9). From the spectra shown in Fig. 8 and 9, a decrease in signal intensity is observed as the absorbed dose increases. In the case of free Macropa, new signals attributed to degradation products also appear. Those signals are observed in the aromatic region between 7 and 8 ppm, as well as in the 2–3 ppm region, which corresponds to protons of the crown-ether. These observations therefore suggest the formation of products involving modifications of both the picolinate arms and the crown-ether framework which is consistent with degradation pathways proposed in Fig. 3. In the case of the La-Macropa complex, except for signals around 2.9 and 1.0 ppm, few new signals appear in the crown-ether region. In contrast, many new peaks emerge in the aromatic region. This suggests that most of the products formed primarily affect the structure of the picolinate arms in the La-Macropa complex as suggested in Fig. 5.

The ^{1}H NMR signals of the free ligand and La-Macropa were integrated between 0 and 30 kGy (Fig. S15–S17 and S22–S24). The amount of undegraded product left is summed up in Table 2.

Each of the signals (Fig. 6 and 7) was integrated separately, after which the mean overall decrease was determined for each received dose (Fig. S16 and S23). The signals of the systems are decreasing with absorbed dose. According to the peak integration, the concentration of Macropa (at pH 5) decreases by 72% at 26.3 kGy, whereas La-Macropa (at pH 6) decreases by only 65% at 28.9 kGy. Because the Macropa and La-Macropa concentration decreases exponentially with absorbed dose, indicative of pseudo-first-order kinetics, the dose constants d and radiolytic yield G_0 can be determined using eqn (6) and (7) from Mincher *et al.*[50]

$$C = C_0 e^{dD} \quad (6)$$

$$G_0 = dC_0/\rho \quad (7)$$

In these equations, C_0 and C are the initial and final concentrations, ρ is the density of the solution, and D is the absorbed dose. Results obtained are summed up in Table 3.

First, it can be noted that the G_0 values obtained are of the same order of magnitude as those reported for other extractants or complexing agents used for actinides and lanthanides.[32–34,36,51–53] Compared with DOTA in similar conditions (aqueous solution with same concentration and dose rate, $G_0 \approx -3$–4×10^{-7} mol J^{-1}), Macropa appears to be more stable, with an estimated G_0 value of -1.25×10^{-7} mol J^{-1}. Thus, Macropa is not expected to generate more degradation products than the reference chelator DOTA. For La-Macropa a G_0 value of -0.76×10^{-7} mol J^{-1} is obtained. Therefore, the complexation of Macropa with a lanthanum ion appears to provide a protective effect.

To summarize, based on ^{1}H NMR and ESI-MS results, Macropa and the Ln-Macropa complex do not follow the same degradation pathway. Free macropa shows a more pronounced degradation than the Ln-complex and mainly involves cleavage of the picolinate arms together with alterations of the crown-ether ring. In contrast, the complex shows improved stability. Moreover, ^{1}H NMR suggests that most of the modifications occur on the picolinate arms. Almost no bond cleavage is observed (except for the minor species **F′**), and the major degradation pathway corresponds to $HO^{\bullet}$ radical attack, leading to the formation of hydroxylated degradation products (+OH).

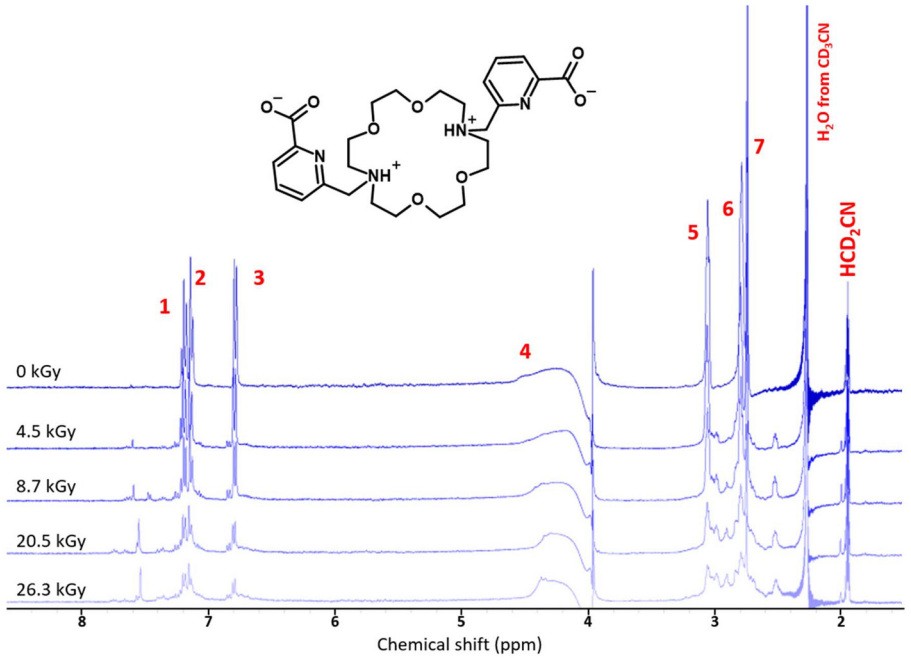

Fig. 8 ^{1}H NMR spectra of non-irradiated and irradiated Macropa solutions. Conditions: 5 × 10^{-3} mol L^{-1} in pure water (pH = 5), 25 °C. CD_3CN is used as external lock solvent and residual undeuterated signal to normalize spectra.

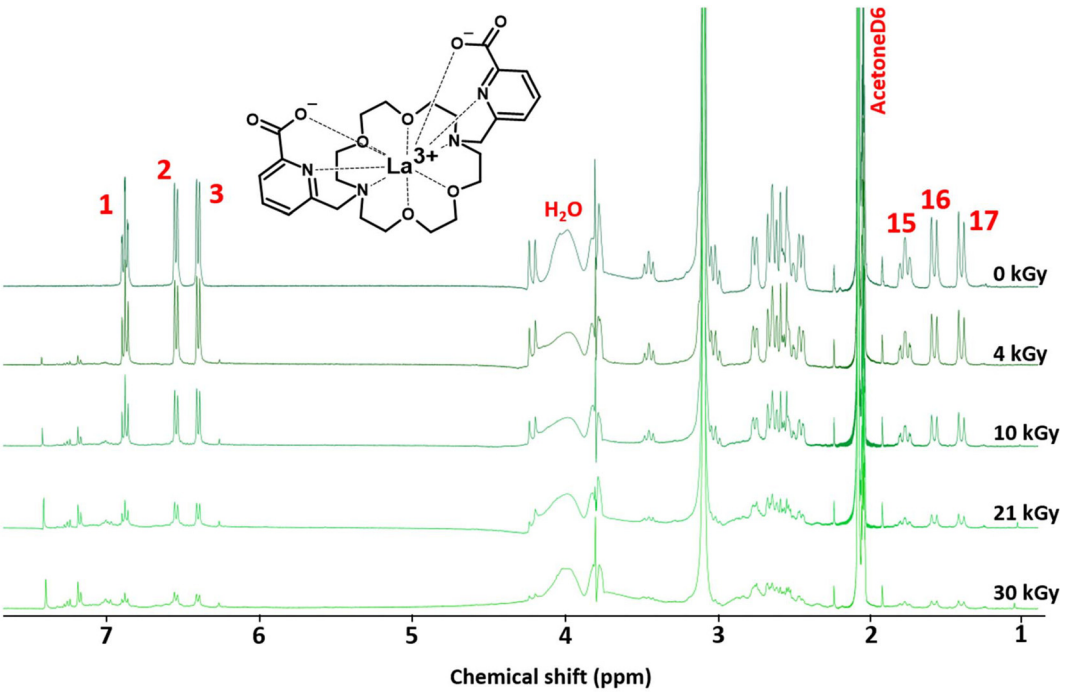

Fig. 9 ^{1}H NMR spectra of non-irradiated and irradiated La-Macropa solutions. Conditions: 5 × 10^{-3} mol L^{-1} in pure water (pH = 6), 25 °C. AcetoneD6 is used as external lock solvent and residual undeuterated signal to normalize spectra.

DFT calculations

Bond dissociation energies (BDE) and Fukui indices were computed for Macropa and La-Macropa. From Fukui indices, it is possible to estimate which atoms have a higher tendency to either loose or accept an electron and are prone to radical attack. From previous studies, it was shown that BDEs and Fukui indices can be simple descriptors to predict the most vulnerable site in the ligand.[45,54] This can be particularly useful to understand the influence of lanthanide complexation

Table 2 Percentage of Macropa and La-Macropa remaining in solution obtained from average NMR signal integration

Irradiation dose (kGy)	0	4.5	8.7	20.5	26.3
Macropa	100%	72%	58%	36%	28%
Irradiation dose (kGy)	0	3.6	9.1	18.6	28.9
La-Macropa pH 6	100%	94%	74%	47%	35%

Table 3 Dose constants (kGy^{-1}) and $-G_0$ values ($\mu mol\ J^{-1}$) for irradiated Macropa and La-Macropa calculated by ^1H NMR signals integration

Sample (x)	pH	d (kGy^{-1})	$-G_0$ (x) (10^{-7} mol J^{-1})
Macropa	5.2	−0.022 ± 0.003	1.25 ± 0.17
La-Macropa	6.0	−0.015 ± 0.002	0.76 ± 0.10

on the radiolysis degradation pathways. Complexation of La by Macropa is expected to change the charge distribution within the molecule and can strengthen or weaken certain bonds.

Calculations were carried out on free Macropa and La-Macropa. The structure of La-Macropa corresponds to the Δ(δλδ)(δλδ) conformer, the geometry of Macropa was optimized starting from the La-Macropa complex, from which the metal cation was removed. It should be noted that an additional water molecule at the eleventh coordination site has been observed in the crystal structure and could be also present in solution as suggested from previous DFT calculations.[18–20] However, its presence should not strongly influence the properties of interest and was not considered in the calculations.

BDEs calculations were done for the C–C and C–N bonds on the picolinate arms (Fig. 10) which were found broken under gamma irradiation only for free Macropa. The results are given in Table 4. For La-Macropa, it is also necessary to break the ionic bond between La^{3+} and the carboxylate group in order to break each C–C and C–N bonds. As a consequence, in the case of La-Macropa, the energy required to cleave both bonds is almost twice as high as for the free chelator. This increased stability is consistent with the experimental observations, since the loss of the carboxylate arm is not observed for La-Macropa.

For Macropa, the energy required to cleave the C–N bond is lower than that for the C–C bond. This result is also consistent with the experimental observations, which show the loss of a picolinate arm before decarboxylation in the case of Macropa (Fig. S12).

Fukui indices were calculated for reactive carbon and nitrogen atoms of Macropa and La-Macropa. Condensed f^0 indices corresponding to radical attack susceptibility are given; atoms with the highest f^0 value are expected to be the most susceptible to radical attack. The highest f^0 values reported in Fig. 11 differ significantly between Macropa and La-Macropa. For La-Macropa, the most reactive C and N atoms correspond to the atoms of the aromatic ring of the picolinate arms. For Macropa the most reactive atom belongs to the crown ether. This is consistent with the observed degradation pathways. For

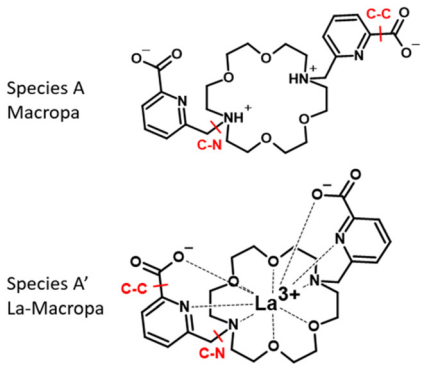

Fig. 10 Bonds studied for Macropa and La-Macropa.

Table 4 Computed bond dissociation energies BDEs (ΔH in kJ mol^{-1}) corresponding to C–C and C–N bond of the picolinate arm for Macropa and La-Macropa as shown in Fig. 10

Bond	Macropa	La-Macropa
C–C	614	1065
C–N	511	1020

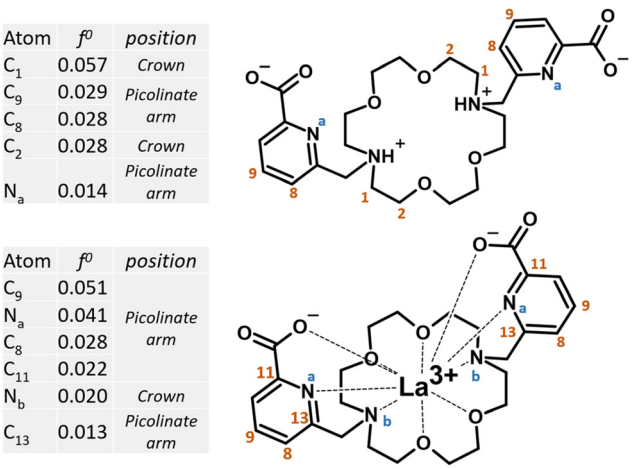

Fig. 11 Calculated Fukui indices (f^0 with absolute value >0.01) for the carbon and nitrogen atoms of the Macropa and La-Macropa complex.

La-Macropa, the major degradation product (**B′**) corresponds to HO˙ radical attack on the aromatic ring. For Macropa, the two primary degradation products correspond to the loss of the picolinate arm (**B**) and to the formation of a double bond on the crown ether (**E**). Both degradation pathways can be initiated with hydrogen abstraction from the most reactive C1 atom. For glycine or DOTA in the presence of HO˙ radical, it has been proposed that the decarboxylation follows hydrogen abstraction from the carbon in the α position to the amine.[35,36] For Macropa, hydroxyl radical addition is only observed on the secondary degradation products **D** and **F**. Fukui indices were computed for species **C** in Fig. S26.

According to f^0 values, as expected, the most reactive atoms belong to the pyridine ring.

Finally, the structures of some products detected on the mass spectra were identified using the DFT calculations. The most likely hydroxyl position on species **B′** was attributed according to the highest f^0 value of La-Macropa. For species **C′**, the position of the second hydroxyl was determined considered the f^0 values for species **B′**. However, it should be noted that the pyridine carbon atoms have similar f^0 value. Moreover, the hydroxyl addition lowers all f^0 values for the carbon atoms, indicating a decreased affinity toward radical attack. The position of the double bond in Macropa degradation product **E** was determined by comparing the energy of several structural isomers, differing in the position of the double bond as shown in Fig. 12. Positions 3 and 5 are not equivalent, as shown in Fig. S30, because of the presence of hydrogen interactions between some of the CH_2 groups and the carboxylate functions. As a result, the optimized geometry exhibits C_2 symmetry. The calculations indicate that the lowest energy corresponds to a double bond located between two carbon atoms of the crown-ether ring at position 3. However, it should be noted that the relative energies of the isomers may not be sufficient to predict the localization of the double bond. Kinetic effects were not considered, although they may play an important role in the hydrogen atom abstraction step.

To conclude, BDE calculations and Fukui indices were computed for the Macropa and La-Macropa systems. The Fukui indices indicate that the carbon atoms from the crown ether are the most likely site for radical attack. However, due to charge redistribution upon lanthanide complexation, the most likely sites shift to the atoms of the pyridine ring, as expected from the experimental results. The BDE results also show that the C–C and C–N bonds of the picolinate arms are significantly stabilized upon complexation with La due to their ionic interaction with La^{3+}.

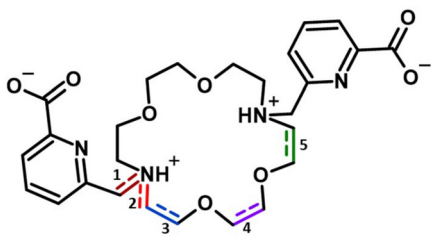

Double bond	ΔE (kJ.mol^{-1})
1 :	+34
2 :	+37
3 :	+0
4 :	+16
5 :	+26

Fig. 12 Energy difference (Δ*E*) between the various positions of the carbon–carbon double bond in the Macropa degradation product *E*. Δ*E* values are given relative to the lowest-energy structural isomer in kJ mol^{-1}.

Conclusion

This study investigated the stability of Macropa and Ln-Macropa systems in water under γ irradiation. According to ESI-MS results, the degradation pathways of Macropa and Ln-Macropa differ. For free Macropa, bond cleavage is observed, particularly involving the picolinate arms. The formation of a hydroxylated species (species **D**) as well as a species featuring a double bond (species **E**) is also detected, but in lower proportions. For the Ln-Macropa complexes, the main degradation products correspond to OH addition to the ligand framework. Based on the ^{1}H NMR spectra this OH addition was proposed to occur predominantly on the picolinate arms. The low proportion of bond cleavage observed for the complex can be explained by the higher energy required to break the C–C and C–N bonds upon complexation, due to the interaction between the metal cation and the coordinating groups located on the picolinate arms. Fukui indices show that, upon lanthanum complexation and charge redistribution, the atomic positions most susceptible to radical attack shift from the crown ether to the pyridine ring.

The determination of the radiolytic degradation yield G_0 shows that free Macropa is already highly resistant to radiolysis. The calculated value of -1.25×10^{-7} mol J^{-1} is lower than that reported for other chelators of medical interest such as DOTA ($\approx -6 \times 10^{-7}$ mol J^{-1}).[34] Moreover, complexation with a large ionic-radius cation such as La^{3+} appears to further improve this stability, with a G_0 value of -0.76×10^{-7} mol J^{-1} for the La-Macropa complex.

Finally, beyond the improved G_0 value observed for the La-Macropa complex, the major degradation products formed do not appear to lose the chelating functions of the ligand. At pH 6, no species corresponding to Macropa that had released La^{3+} was detected, indicating that the complexation properties are preserved. This is a critical requirement for the use of such chelators in nuclear medicine. Future studies are underway in which an alpha emitter (^{241}Am) will be introduced into solution to assess how the type of radiation influences the degradation products formed.

Conflicts of interest

There are no conflicts to declare.

Data availability

The data supporting this article have been included as part of the supplementary information (SI). Supplementary information: HPLC, ESI-MS and NMR spectra of Tb-Macropa and La-Macropa complexes, Fukui indices of Macropa and La-Macropa from DFT calculations. See DOI: https://doi.org/10.1039/d6dt00671j.

References

1 T. I. Kostelnik and C. Orvig, *Chem. Rev.*, 2019, **119**, 902–956.
2 M. L. Grieve and B. M. Paterson, *Aust. J. Chem.*, 2021, **75**, 65–88.
3 M. Miederer, M. Benešová-Schäfer, C. Mamat, D. Kästner, M. Pretze, E. Michler, C. Brogsitter, J. Kotzerke, K. Kopka, D. A. Scheinberg and M. R. McDevitt, *Pharmaceuticals*, 2024, **17**, 76.
4 K. A. Morgan, S. E. Rudd, A. Noor and P. S. Donnelly, *Chem. Rev.*, 2023, **123**, 12004–12035.
5 S. Salih, A. Alkatheeri, W. Alomaim and A. Elliyanti, *Molecules*, 2022, **27**, 5231.
6 E. Aluicio-Sarduy, N. A. Thiele, K. E. Martin, B. A. Vaughn, J. Devaraj, A. P. Olson, T. E. Barnhart, J. J. Wilson, E. Boros and J. W. Engle, *Chem. – Eur. J.*, 2020, **26**, 1238–1242.
7 A. Hu and J. J. Wilson, *Acc. Chem. Res.*, 2022, **55**, 904–915.
8 A. Hu, M. E. Simms, V. Kertesz, J. J. Wilson and N. A. Thiele, *Inorg. Chem.*, 2022, **61**, 12847–12855.
9 R. Eychenne, M. Chérel, F. Haddad, F. Guérard and J.-F. Gestin, *Pharmaceutics*, 2021, **13**, 906.
10 K. A. Deal, I. A. Davis, S. Mirzadeh, S. J. Kennel and M. W. Brechbiel, *J. Med. Chem.*, 1999, **42**, 2988–2992.
11 L. Li, J. Rousseau, M. de G. Jaraquemada-Peláez, X. Wang, A. Robertson, V. Radchenko, P. Schaffer, K.-S. Lin, F. Bénard and C. Orvig, *Bioconjugate Chem.*, 2021, **32**, 1348–1363.
12 M. Essler, F. C. Gärtner, F. Neff, B. Blechert, R. Senekowitsch-Schmidtke, F. Bruchertseifer, A. Morgenstern and C. Seidl, *Eur. J. Nucl. Med. Mol. Imaging*, 2012, **39**, 602–612.
13 M. R. McDevitt, D. Ma, J. Simon, R. K. Frank and D. A. Scheinberg, *Appl. Radiat. Isot.*, 2002, **57**, 841–847.
14 M. Miederer, G. Henriksen, A. Alke, I. Mossbrugger, L. Quintanilla-Martinez, R. Senekowitsch-Schmidtke and M. Essler, *Clin. Cancer Res.*, 2008, **14**, 3555–3561.
15 N. A. Thiele, V. Brown, J. M. Kelly, A. Amor-Coarasa, U. Jermilova, S. N. MacMillan, A. Nikolopoulou, S. Ponnala, C. F. Ramogida, A. K. H. Robertson, C. Rodríguez-Rodríguez, P. Schaffer, C. Williams Jr., J. W. Babich, V. Radchenko and J. J. Wilson, *Angew. Chem., Int. Ed.*, 2017, **56**, 14712–14717.
16 K. A. Morgan, C. W. Wichmann, L. D. Osellame, Z. Cao, N. Guo, A. M. Scott and P. S. Donnelly, *Chem. Sci.*, 2024, **15**, 3372–3381.
17 D. J. Fiszbein, V. Brown, N. A. Thiele, J. J. Woods, L. Wharton, S. N. MacMillan, V. Radchenko, C. F. Ramogida and J. J. Wilson, *Inorg. Chem.*, 2021, **60**, 9199–9211.
18 A. Kovács, *ACS Omega*, 2020, **5**, 26431–26440.
19 A. Kovács and Z. Varga, *Struct. Chem.*, 2021, **32**, 643–653.
20 M. K. Blei, L. Waurick, F. Reissig, K. Kopka, T. Stumpf, B. Drobot, J. Kretzschmar and C. Mamat, *Inorg. Chem.*, 2023, **62**, 20699–20709.
21 Y. Liu, C.-Z. Wang, Q.-Y. Wu, J.-H. Lan, Z.-F. Chai, W.-S. Wu and W.-Q. Shi, *Inorg. Chem.*, 2022, **61**, 4404–4413.
22 A. Roca-Sabio, M. Mato-Iglesias, D. Esteban-Gómez, É. Tóth, A. de Blas, C. Platas-Iglesias and T. Rodríguez-Blas, *J. Am. Chem. Soc.*, 2009, **131**, 3331–3341.
23 M. P. Jensen, R. Chiarizia, I. A. Shkrob, J. S. Ulicki, B. D. Spindler, D. J. Murphy, M. Hossain, A. Roca-Sabio, C. Platas-Iglesias, A. de Blas and T. Rodríguez-Blas, *Inorg. Chem.*, 2014, **53**, 6003–6012.
24 A. E. Kynman, A. N. Dang, T. S. Grimes, S. P. Mezyk, J. R. Wilbanks, C. A. Zarzana, R. G. Deokar, A. R. Cook, D. Boglaienko, G. B. Hall and G. P. Horne, *ACS Omega*, 2025, **10**, 7822–7830.
25 S. P. Mezyk, M. Baxter, C. Celis-Barros, T. S. Grimes, P. R. Zalupski, C. Rae, C. A. Zarzana, A. R. Cook and G. P. Horne, *Dalton Trans.*, 2024, **53**, 6881–6891.
26 G. P. Horne, C. Celis-Barros, J. K. Conrad, T. S. Grimes, J. R. McLachlan, B. M. Rotermund, A. R. Cook and S. P. Mezyk, *Phys. Chem. Chem. Phys.*, 2023, **25**, 16404–16413.
27 A. E. Kynman, T. S. Grimes, A. R. Cook, D. R. Peterman and G. P. Horne, *Radiat. Phys. Chem.*, 2026, **239**, 113246.
28 V. V. Makhlyarchuk and S. V. Zatonskii, *Russ. Chem. Rev.*, 1992, **61**, 484–499.
29 C. C. Barros, C. D. Pilgrim, A. R. Cook, S. P. Mezyk, T. S. Grimes and G. P. Horne, *Phys. Chem. Chem. Phys.*, 2021, **23**, 24589–24597.
30 T. Toigawa, D. R. Peterman, D. S. Meeker, T. S. Grimes, P. R. Zalupski, S. P. Mezyk, A. R. Cook, S. Yamashita, Y. Kumagai, T. Matsumura and G. P. Horne, *Phys. Chem. Chem. Phys.*, 2021, **23**, 1343–1351.
31 A. Kimberlin, G. Saint-Louis, D. Guillaumont, B. Camès, P. Guilbaud and L. Berthon, *Phys. Chem. Chem. Phys.*, 2022, **24**, 9213–9228.
32 S. N. Bhattacharyya and K. P. Kundu, *Int. J. Radiat. Phys. Chem.*, 1972, **4**, 31–41.
33 N. E. Bibler, *J. Inorg. Nucl. Chem.*, 1972, **34**, 1417–1425.
34 I. Mahti, D. Guillaumont, C. Berthon, G. Saint-Louis, X. Hérès and L. Berthon, *Dalton Trans.*, 2023, **52**, 9952–9963.
35 E. Avraham, D. Meyerstein, A. Lerner, G. Yardeni, S. Pevzner, I. Zilbermann, P. Moisy, E. Maimon and I. Popivker, *Free Radicals Biol. Med.*, 2022, **180**, 134–142.
36 V. Fiegel, C. Berthon, A. Costagliola, G. Blain, J. Vandenborre, J. Vermeulen, G. Saint-Louis, L. Guerin, T. Sauvage, M. Fattahi-Vanani, L. Venault and L. Berthon, *Radiat. Phys. Chem.*, 2019, **165**, 108409.
37 F. H. Attix, W. C. Roesch and E. Tochilin, *Radiation dosimetry*, Academic Press, New York, 1966.
38 E. L. Hooijman, J. R. de Jong, C. M. Ntihabose, F. Bruchertseifer, A. Morgenstern, Y. Seimbille, T. Brabander, S. L. W. Koolen and E. de Blois, *EJNMMI Radiopharm. Chem.*, 2025, **10**, 9.
39 E. L. Hooijman, V. Radchenko, S. W. Ling, M. Konijnenberg, T. Brabander, S. L. W. Koolen and E. de Blois, *EJNMMI Radiopharm. Chem.*, 2024, **9**, 9.
40 E. Demirci, N. Alan Selçuk, G. Beydağı, M. Ocak, T. Toklu, K. Akçay and L. Kabasakal, *Mol. Imaging Radionucl. Ther.*, 2023, **32**, 226–232.

41 M. J. Frisch, G. W. Trucks, H. B. Schlegel, G. E. Scuseria, M. A. Robb, J. R. Cheeseman, G. Scalmani, V. Barone, G. A. Petersson and H. Nakatsuji, *Gaussian 16*, Gaussian, Inc., Wallingford, CT, 2016.
42 M. Dolg, H. Stoll, A. Savin and H. Preuss, *Theor. Chim. Acta*, 1989, **75**, 173–194.
43 A. D. Becke, *J. Chem. Phys.*, 1993, **98**, 5648–5652.
44 J. P. Perdew, *Phys. Rev. B: Condens. Matter Mater. Phys.*, 1986, **33**, 8822–8824.
45 A. Smirnova, A. Mitrofanov, P. Matveev, T. Baygildiev and V. Petrov, *Phys. Chem. Chem. Phys.*, 2020, **22**, 14992–14997.
46 T. Koubský and J. Luštinec, *J. Radioanal. Nucl. Chem.*, 2018, **318**, 2407–2413.
47 E. Glendening, A. Reed, J. Carpenter and F. Weinhold, NBO 3.1N.
48 J. I. Mujika, J. Uranga and J. M. Matxain, *Chem. – Eur. J.*, 2013, **19**, 6862–6873.
49 N. G. Luk'yanenko, A. V. Lobach, M. N. Parfenova, L. N. Lyamtseva, O. S. Timofeev and A. I. Gren', *Chem. Heterocycl. Compd.*, 1987, **23**, 940–943.
50 B. J. Mincher and R. D. Curry, *Appl. Radiat. Isot.*, 2000, **52**, 189–193.
51 S. N. Bhattacharyya and E. V. Srisankar, *Int. J. Radiat. Phys. Chem.*, 1976, **8**, 667–671.
52 B. K. Sharma and R. Gupta, *Radiat. Eff.*, 1981, **57**, 149–154.
53 K. Krapfenbauer and N. Getoff, *Radiat. Phys. Chem.*, 1999, **55**, 385–393.
54 P. I. Matveev, A. A. Mitrofanov, V. G. Petrov, S. S. Zhokhov, A. A. Smirnova, Y. A. Ustynyuk and S. N. Kalmykov, *RSC Adv.*, 2017, **7**, 55441–55449.